Biosensors and Bioelectronics 143 (2019) 111602

Contents lists available at ScienceDirect

Biosensors and Bioelectronics

journal homepage: www.elsevier.com/locate/bios

Triple-helix molecular switch-based versatile "off-on" electrochemiluminescence and fluorescence biosensing platform for ultrasensitive detection of lipopolysaccharide by multiple-amplification strategy

Xiaoshan Gao, Hongkun Li, Yu Zhao, Guifen Jie*

Key Laboratory of Optic-electric Sensing and Analytical Chemistry for Life Science, MOE, Shandong Key Laboratory of Biochemical Analysis, Key Laboratory of Analytical Chemistry for Life Science in Universities of Shandong, College of Chemistry and Molecular Engineering. Qingdao University of Science and Technology, Qingdao, 266042, PR China

ARTICLE INFO

Keywords:
Triple-helix molecular
$CdTe–Ru@SiO_2$
Multiple-amplification strategy
ECL

ABSTRACT

Herein, a novel biosensing platform for versatile electrochemiluminescence (ECL) "off" and fluorescence (FL) "on" detection of lipopolysaccharide (LPS) with multiple-amplification strategy is proposed. The specific recognition of target to aptamer on the magnetic beads (MB) firstly released abundant DNA sequences of three kinds. The sequences hybridized with multifunctional molecular beacon (MMB) and initiated numerous bidirectional polymerization and shearing reactions, generating a large number of DNA fragments (a1) by multiple cycling amplification. Then a1 was introduced to the triple-helix sensing system, opening the triple-helix structure. In ECL system, the G-rich chains S2 were exposed to form G-quadruplex-hemin complex in the presence of hemin, which could efficiently quench ECL for "off" detection of LPS. In FL system, the fluorophore FAM and quencher BHQ on S1 chain were separated with opening of triple-helix structure, achieving fluorescence "on" signal for LPS assay. So the versatile platform can achieve greatly amplified ECL and FL signal changes for sensitive assay of LPS, showing wide linear ranges (0.1 fg/mL-0.1 ng/mL by ECL and 10 fg/mL^{-1}-1 μg/mL by FL) and low detection limits (0.012 fg/mL by ECL and 1.269 fg/mL by FL). Therefore, the present ECL "Off" and FL "On" dual-signal detection patterns for LPS displayed many advantages over other reported methods, which provided an outlook for future applications in clinical diagnosis.

1. Introduction

DNA nanotechnology is a fast-growing research field (Wilner and Willner, 2012; Zhang and Seelig, 2011). Nucleic acid base sequences are often encoded to construct one-, two-, and three-dimensional DNA nanostructures (Torring et al., 2011), such as DNA switches (Wang et al., 2015), DNA machines (Liu et al., 2014) and DNA logic-gate operations (Willner et al., 2008). The nanostructure of triple nucleic acid has attracted people's attention. Triple DNA is used as an identification element and a functional structure switching unit that allows an output signal to be generated upon target recognition. Triplex DNA structures were applied as central elements for further developing DNA nanotechnology and nucleic acid-based functional materials. These results reflect the importance of DNA triplex in future medicine and greatly contribute to the biological significance of these systems (Zain and Sun, 2003).

Electrochemiluminescence (ECL) displayed excellent controllability and sensitivity (Liu et al., 2015), and has been applied in food detection (Ge et al., 2019a), environmental monitoring (Cai et al., 2015) and clinical treatment (Zhang et al., 2016). People's research on ECL has involved practical applications in biological and chemical analysis (Liu et al., 2015; Jie et al., 2018; Li et al., 2017; Wen et al., 2017; Du and Dong, 2017). Quantum dots (QDs)-based ECL sensors have been widely applied for analytical detection of some analytes (Khonsari and Sun, 2017, 2018). People made significant efforts to increase the intensity of ECL sensors to detect trace amounts of target molecules more sensitively (Ge et al., 2019b; Li et al., 2019). Since the ECL intensity is largely dependent on the electron transfer efficiency between illuminant and co-reactant, intramolecular self-reinforcing ECL emitter is demonstrated by covalently binding the co-reactant to the ECL illuminant (Zhuo et al., 2014). Intramolecular reactions reduce the electron transport distance and complexity of interaction between free radical

* Corresponding author.
E-mail address: guifenjie@126.com (G. Jie).

https://doi.org/10.1016/j.bios.2019.111602
Received 29 June 2019; Received in revised form 7 August 2019; Accepted 13 August 2019
Available online 14 August 2019
0956-5663/

intermediate reactants to improve the sensing sensitivity (Swanick et al., 2012; Zhuo et al., 2014; Liang et al., 2015; Wang et al., 2016a; Wang et al., 2016b; Carrara et al., 2017). In addition, fluorescent probes are widely used in biochemical assays, the biochemical event can cause obvious fluorescence signal change by controlled fluorophore-quencher distance (Lee et al., 1993).

Lipopolysaccharide (LPS) is a major component in the outer cell membrane of Gram-negative bacteria (Ulevitch and Tobias, 1994) and is highly toxic at low concentrations (Warren et al., 2010). In recent years, people have made a lot of efforts in developing high-sensitivity detection of LPS, and achieved remarkable results (Rangin and Basu, 2004; Voss et al., 2007). Although the sensitivity to LPS detection has been greatly improved, detection at picomolar concentrations still faces serious challenges.

In this work, the triplex nucleic acids molecular beacon was used to induce two signal responses of both ECL and FL to achieve high sensitive detection of LPS. On the one hand, the novel intramolecular reinforcing material CdTe–Ru@SiO_2 was used as signal response, showing very strong ECL intensity. In the presence of LPS, the change of triple-helix structure induce formation of G-quadruplex-hemin complex, producing an “on” to “off” ECL signal response for target LPS assay. On the other hand, the energy transfer of fluorophore and quencher was used to trigger response change of fluorescence signal. In the absence of LPS, the triple-helix structure caused the proximity of fluorophore and the quencher, and the fluorescence signal was “off” state. Introducing the target LPS, the triple-helix structure was opened, the fluorophore and quencher was separated, so the signal response was “on” state. The present method can enable accurate dual detection of LPS by ECL and FL, showing high sensitivity and selectivity, which can provide promising applications for clinical diagnosis.

2. Experimental section

2.1. Preparation of CdTe–Ru@SiO_2 nanospheres

Firstly, the CdTe QDs were prepared. $NaBH_4$ (50.0 mg) and Te powder (80.0 mg) were added to ultrapure water for 30 min at 45 °C in nitrogen gas environment. The solution turns dark purple and the clear NaHTe solution was obtained after Te powder disappeared completely (Gu et al., 2008). Meanwhile, 2.5 mmol of $CdCl_2$ was dissolved into 63 mL of ultrapure water, followed by adding 55 μL of 3-mercaptopropionic acid (MPA), and the pH was adjusted to 9.0 with 0.2 mol L^{-1} NaOH. (In the process, the clear solution firstly turned turbid, and then became clear again, so NaOH was added slowly to avoid excess). Then NaHTe solution (250 μL) was injected into the $CdCl_2$ reaction flask and heated to 130 °C (at this point the solution is boiling) and refluxed for 12 h. Finally, the orange red CdTe QDs solution was obtained.

The CdTe–Ru@SiO_2 was prepared according to synthesis method for Ru@SiO_2 nanospheres (Zhang and Dong, 2006; Wang et al., 2016c). The CdTe QDs (200 μL) react with $[Ru(bpy)_3]^{2+}$ (80 mM, 170 μL) for 12 h, ($[Ru(bpy)_3]^{2+}$ complex electrostatically attracts MPA by the opposite charge), and then cyclohexane, TX-100 and n-hexanol were add to the above conical flask for 25 min. Next, the precursor tetraethyl orthosilicate (TEOS) (100 μL), 60 μL of $NH_3{\cdot}H_2O$ was added. After the reaction was placed for 24 h with a dark environment, the products were isolated with acetone, centrifuged (12000 rpm, 10 min) and purified with ethanol. The purified CdTe–Ru@SiO_2 was dispersed in PBS solution.

2.2. Preparation of aptamer modified magnetic beads

100 μL of magnetic beads were washed three times with 500 μL of PBS (0.1 M, pH 7.4, containing 0.1 M KCl). Then carboxyl groups were activated in 200 μL of 0.1 M PBS containing 10 mg of N-Hydroxysuccinimide (NHS) and 20 mg of 1-(3-Dimethylaminopropyl)-3-ethylcarbodiimide hydrochloride (EDC) for 1 h at room temperature, and the supernatant was discarded. (Liu and Lu, 2006; Yu et al., 2016). After that, 100 μL of 1.0 μM LPS aptamer was added to the activated magnetic beads solution to react for 6 h at 37 °C in a constant temperature oscillator. After magnetic separation, the aptamer-magnetic beads were dispersed in 200 μL of 0.1 M PBS and incubated at 37 °C for 1 h. Next, 300 μL of three kinds of mDNA (10^{-5} M for each) were added to the above solution and incubated at 37 °C for 2 h. After washing with PBS, the final reaction was resuspended in 200 μL of PBS (0.1 M, pH 7.4). The final aptamer-mDNA-magnetic beads solution was stored at 4 °C.

2.3. Target cyclic amplification reaction

The mixture of specified concentration of LPS (15 μL) and the aptamer magnetic beads hybridization solution (10 μL) was incubated for 2 h to release m1, m2, m3. The m1, m2, and m3 were left in the supernatant after magnetic separation. Then 2.5 μL of 10 × NE buffer 2, 0.5 μL of 0.1 μM MMB, 0.6 μL of Klenow fragment (3′–5′ exo-, 5 U/μL), 0.6 μL of Nt.BbvCI nickase (10 U/μL), 1 μL of dNTPs (10 mM), and 20 μL of the supernatant were added into eppendorf tube. The reaction was terminated at 80 °C for 20 min after the mixture was incubated at 37 °C for 90 min. At this point, the solution contains a large amount of replaced nicked fragments (a1).

2.4. Formation of triple-helix DNA

DNA S1 (5.0 μL, 10 μM) and DNA S2 (50 μL, 1.0 μM) were added to 45 μL incubation buffer (10 mM PB, 20 mM NaCl, 2.5 mM $MgCl_2$, pH 5.2) and incubated for 2 h to form the triple-helix DNA.

2.5. ECL detection of LPS

The gold electrodes (GEs) were polished with 1.0, 0.3 and 0.05 μm alumina powder and rinsed with ultrapure water. Then, the electrodes were ultrasonically treated in 50% methanol solution for 3 min. Subsequently, 10 μL of CdTe–Ru@SiO_2 solution was dropped on the bare GEs surface and dried. Then the electrodes were immersed in EDC/NHS (20 mg mL^{-1}/10 mg mL^{-1}) solution for 20 min to activate carboxyl groups, and rinsed with ultrapure water. Subsequently, the electrodes were immersed in triple-helix DNA solution for 6 h, being rinsed with ultrapure water. After the modified electrode was blocked with 1 mM mercaptohexanol (MCH) for 2 h, the electrodes were immersed in the replaced nicked fragments (a1) for 2 h, then being rinsed with ultrapure water. Finally, 10 μL of hemin ($7*10^{-4}$ M) was pipetted onto the modified electrodes for 30 min, to form hemin/G-quarduplex nanostructure. The modified electrodes were rinsed with ultrapure water and dried in air. ECL detection solution was PBS solution (0.1 M, pH = 7.4) containing 10 mM TPrA. The scanning potential, scanning rate and the photomultiplier tube is from 0.2 to 1.25 V, 0.1 V/s and -500 V, respectively.

2.6. Fluorescence detection of LPS

100 μL of carboxyl-modified magnetic beads were washed with 0.5 mL PBS (0.1 M, pH 7.4, with 0.1 M KCl). Then magnetic beads were activated in EDC/NHS (20 mg mL^{-1}/10 mg mL^{-1}) solution for 20 min with gentle shaking, then the supernatant was discarded. Subsequently, triple-helix DNA solution was added to the activated magnetic beads solution with gentle shaking for 6 h, the supernatant was discarded. Finally, the replaced nicked fragments (a1) were added to the modified magnetic beads solution with gentle shaking for 2 h. The reserved supernatant was used for fluorescence detection after magnetic separation.

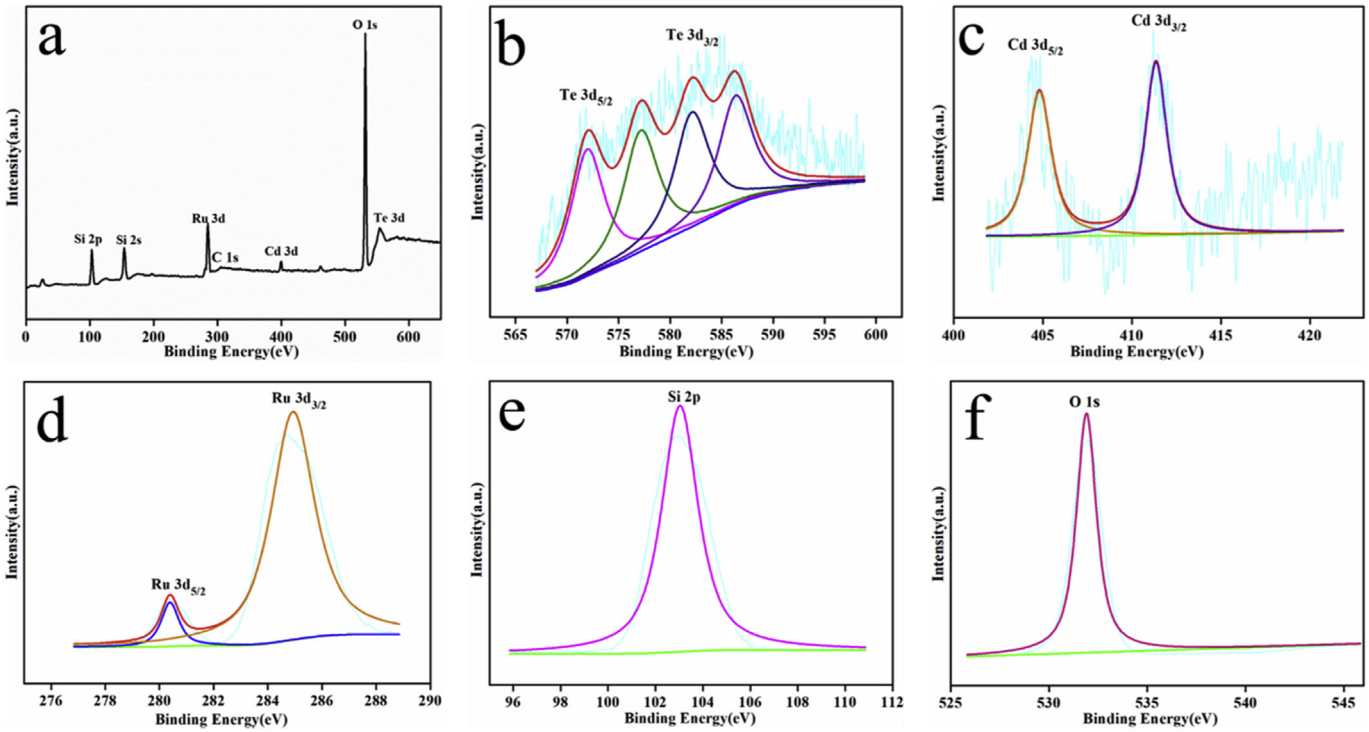

Fig. 1. X-ray photoelectron spectra of CdTe–Ru@SiO_2 nanospheres (a) and corresponding Te 3d (b), Cd 3d (c), Ru 3d (d), Si 2p (e), and O 1s (f) states.

3. Results and discussion

3.1. Characterization of the CdTe–Ru@SiO_2 nanospheres

X-ray photoelectron spectroscopy (XPS) is used to confirm the element composition of the prepared CdTe–Ru@SiO_2 nanospheres (Fig. 1). The characteristic peaks including Te $3d_{5/2}$ at 572.3 eV, Cd $3d_{5/2}$ at 403.1 eV, and Ru $3d_{5/2}$ at 280.5 eV can confirm that the nanospheres have tellurium, cadmium, and ruthenium species. In addition, Si 2p, O 1s are also observed.

Fig. 2A showed the high resolution transmission electron micrograph (HRTEM) image of CdTe–Ru@SiO_2 nanospheres, the uniform spherical morphology was observed, and the average diameter of nanospheres was about 43 nm. Many nanoparticles of CdTe QDs were distributed over the nanospheres. Fig. 2B displayed the fluorescence (FL) spectra of CdTe–Ru@SiO_2 nanospheres, the emission peak at 591 nm is high (Excitation wavelength: 469 nm), indicating that the CdTe–Ru@SiO_2 nanospheres have good FL property.

Fig. 2C showed SEM image of CdTe–Ru@SiO_2 nanospheres, it can be seen that the nanospheres are evenly distributed and their size matches TEM image. Fig. 2D displayed the X-ray powder diffraction (XRD) pattern of the CdTe–Ru@SiO_2 nanospheres, the diffraction peaks of the powder perfectly match CdTe QDs standard cards (JCPDS 89–3053, and JCPDS 89–3434). The three characteristic peaks (red) of CdTe QDs appearing at 23.76°, 39.29°, and 46.44° correspond to three lattice planes (111), (220) and (311), respectively. The four characteristic peaks (black) of SiO_2 nanopheres appearing at 22.05°, 28.53°, 31.54° and 36.20° correspond to four lattice planes (101), (111), (102) and (200). In addition, since Ru exists in the form of ions, the absorption peak of Ru is not shown in XRD, but in the XPS spectrum, the presence of Ru can be seen.

Fig. 2E showed the FTIR spectra of CdTe–Ru@SiO_2 nanospheres, the peaks at around 3420, 2930, 1640, 1360, and 587 cm^{-1} are ascribed to υ (OH), υ (CH_2), υ (C═O), υ (C–O), and δ (C–S), which are the characteristic peaks of MPA. However, the S–H vibration (around 2550 cm^{-1}) is not detectable, which is speculated that thiols are covalently bound to the surface of the QDs, indicating the existence of CdTe QDs (Chang et al., 2019). The strong and wide absorption band of 1110 cm^{-1} is the υ (Si–O–Si), and the peak at 830 cm^{-1} is the υ (Si–O), indicating the presence of SiO_2 (Cho et al., 2019). In addition, the peaks of 1470 cm^{-1} and 1510 cm^{-1} are the skeleton vibration absorption peaks of C═N and C═C of bipyridine, and the peak corresponding to 1250 cm^{-1} is the in-plane bending vibration peak of bipyridine, indicating the existence of Ru (Omberg et al., 1997).

Fig. 2F showed HRTEM image of CdTe QDs, the uniform nanoparticles of QDs with an average diameter of about 3 nm were observed.

3.2. Electrochemiluminescence of the CdTe–Ru@SiO_2 nanospheres

The CdTe–Ru@SiO_2 displays high ECL intensity (Fig. S1A). A strong ECL peak at positive potential (+1.5 V) is observed on the ECL - potential curve, which is due to reaction of CdTe–Ru@SiO_2 with the coreactant TPrA. In particular, CdTe–Ru complex is encapsulated in the SiO_2 nanospheres, after deprotonation process, the TPrA radicals react with $[Ru(bpy)_3]^{3+}$, generating $[Ru(bpy)_3]^{2+}$*(eq (4)). QDs are excited due to energy transfer between $[Ru(bpy)_3]^{2+}$* and CdTe QDs (eq (5)). The electron transfer path between $[Ru(bpy)_3]^{2+}$* and CdTe QDs is greatly shortened and the RET efficiency is improved. According to the previous mechanisms (Miao et al., 2002; Dong et al., 2015), the ECL-RET process is described as follows:

$$[Ru(bpy)_3]^{2+} - e^- \rightarrow [Ru(bpy)_3]^{3+} \quad (1)$$

$$TPrA - e^- \rightarrow TPrA^{+\bullet} \quad (2)$$

$$TPrA^{+\bullet} \rightarrow TPrA^{\bullet} + H^+ \quad (3)$$

$$TPrA^{\bullet} + [Ru(bpy)_3]^{3+} \rightarrow [Ru(bpy)_3]^{2+}* + \text{products} \quad (4)$$

$$[Ru(bpy)_3]^{2+}* + CdTe \rightarrow [Ru(bpy)_3]^{2+} + CdTe* \quad (5)$$

$$CdTe* \rightarrow CdTe + hv \quad (6)$$

Fig. S1B shows ECL of the CdTe–Ru@SiO_2 nanospheres under continuous cyclic voltammetry scan, the ECL signals are high and steady, indicating that the CdTe–Ru@SiO_2 nanospheres can be used as an excellent ECL probe for further biosensing analysis.

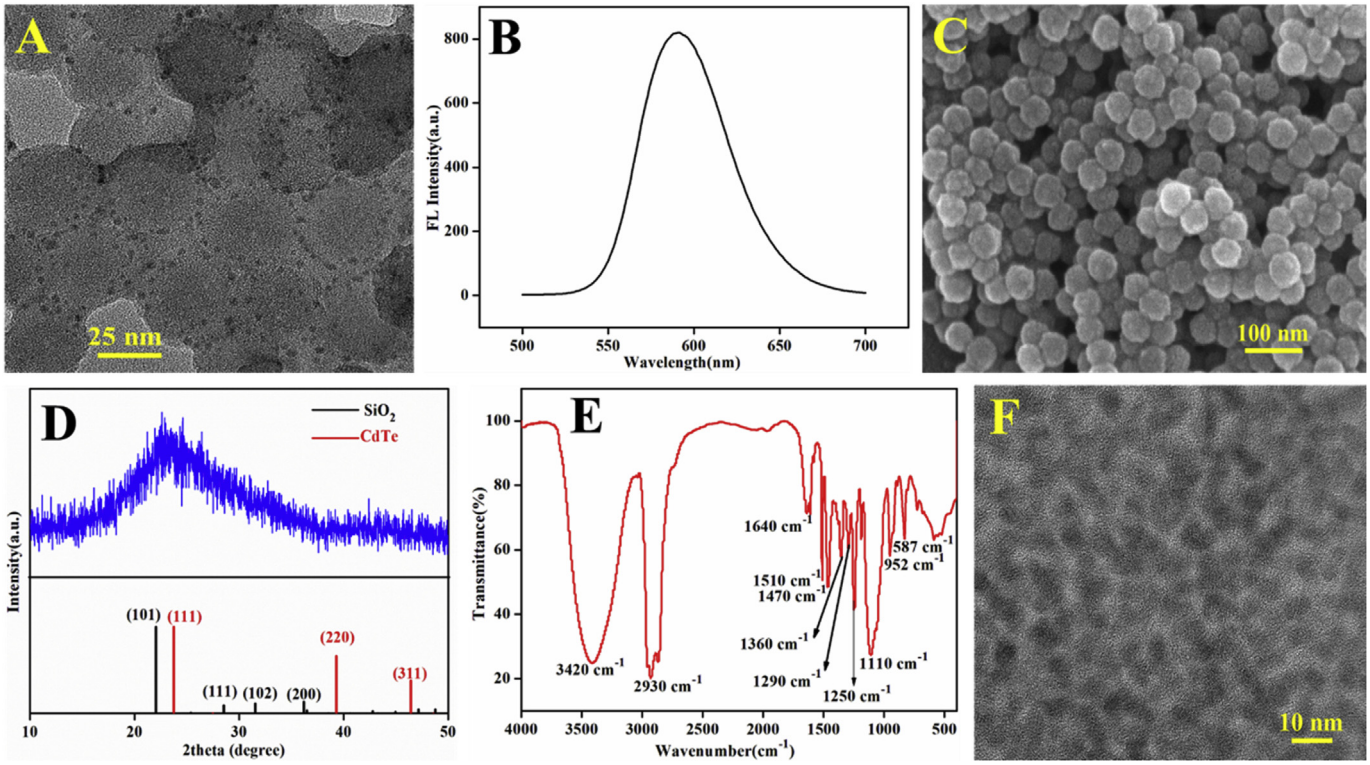

Fig. 2. (A) HRTEM image, (B) FL spectra, (C) Scanning electron microscopy (SEM) image, (D) XRD spectra, (E) FTIR spectra of the CdTe–Ru@SiO_2 nanospheres; (F) HRTEM image of CdTe QDs.

3.3. Principle for ECL "On − Off" and fluorescence "Off − On" detection of LPS

Scheme 1 shows the principle of ECL and FL dual-signal biosensing platform for LPS detection by multiple-amplification process. Scheme 1A is the release process of DNA sequences (m1, m2, m3) triggered by target LPS. Scheme 1B is the multiple cyclic amplification process in which m1, m2, m3 and MMB molecules are combined by geometric progression for generating abundant DNA fragments. Scheme 1C is the principle for dual detection of LPS by ECL "Off" and fluorescence "On" signals based on the triple helix molecular switch.

As shown in Scheme 1A, the hybridized LPS aptamer-mDNA is firstly linked to the magnetic beads via amide bond, then the specific binding of target LPS to its aptamer led to release of DNA m1, m2, m3. The DNA sequences (m1, m2, m3) include two parts which are complementary to LPS aptamer and MMB, respectively. As shown in Scheme 1B, MMB is firstly in stem-loop structure state. When m1, m2, m3 are introduced to hybridize with MMB, the MMB structure is opened by geometric progression, resulting in bi-directionally extended MMB/extended MMB duplex (EM-duplex) and release of m1, m2, m3 by polymerization, then m1, m2, and m3 are recycled by binding to another MMB. Subsequently, with the help of Klenow fragment and Nt.BbvCI nickase, a series of polymerization and nicked reaction are initiated and proceeded repeatedly, which leads to accumulation of large amounts of a1. As shown in Scheme 1C, the triple-helix structure is firstly formed between S1 labeled with FAM and BHQ and S2 by Watson-Crick and Hoogsteen base pairings. The triple-helix structure molecules with amino groups on S2 are linked to the magnetic beads by amido bond. As FAM and BHQ are close in the triple-helix structure, the fluorescence signal is "off" state by energy transfer.

When the target-generated single strands a1 are present, S1 in the triple-helix structure is opened by hybridization to separate FAM and BHQ, achieving fluorescence signal "on" state for sensitive detection of target LPS. In addition, the triple-helix structure is assembled on the electrode surface through amide bond, when the present a1 hybridizes with S1, the G-rich chains S2 are exposed. With the help of hemin, the formed G-quadruplex-hemin complex can quench ECL by consuming luminescent excitation state and increase of electron transfer resistance, which results in "off" ECL signal for LPS assay.

3.4. Quenching mechanism investigation of the CdTe–Ru@SiO_2 nanospheres ECL system

The quenching mechanism of CdTe–Ru@SiO_2 nanospheres by hemin was explored. After hemin is added, the ECL intensity exhibited a sharp decrease from 17050 au (curve a) to 1025 au (curve b) (Fig. S2A). The ECL quenching mechanism is speculated: hemin (Fe^{II}) is oxidized to hemin (Fe^{III}) (eq (7)), then hemin (Fe^{III}) can compete with $[Ru(bpy)_3]^{3+}$ to react with $TPrA^{\bullet}$ (eq (8)). Moreover, electron transfer occur between CdTe QDs^{+*} and hemin (Fe^{III}), producing CdTe QDs $(h)^+$ (eq (10)) or between $[Ru(bpy)_3]^{2+*}$ and hemin (Fe^{III}) to produce $[Ru(bpy)_3]^{3+}$ (eq (9)). According to the previous mechanisms (Zhao et al., 2017), the possible ECL quenching mechanisms are outlined as the following equations:

$$\text{hemin } (Fe^{II}) - e \rightarrow \text{hemin } (Fe^{III}) \quad (7)$$

$$\text{hemin } (Fe^{III}) + TPrA^{\bullet} \rightarrow \text{hemin } (Fe^{II}) + \text{products} \quad (8)$$

$$\text{hemin } (Fe^{III}) + [Ru(bpy)_3]^{2+*} \rightarrow \text{hemin } (Fe^{II}) + [Ru(bpy)_3]^{3+} \quad (9)$$

$$\text{hemin } (Fe^{III}) + \text{CdTe } QDs^{+*} \rightarrow \text{hemin } (Fe^{II}) + \text{CdTe QDs } (h)^+ \quad (10)$$

In addition, the steric hindrance of hemin/G-quadruplex also result in the decrease in ECL intensity, which is another reason for quenching ECL signal.

3.5. Feasibility analysis of the biosensing platform for LPS detection

The feasibility for LPS detection was investigated, the control experiments in the absence/presence of LPS were carried out to confirm the analysis. As shown in Fig. S2B, the CdTe–Ru@SiO_2 modified

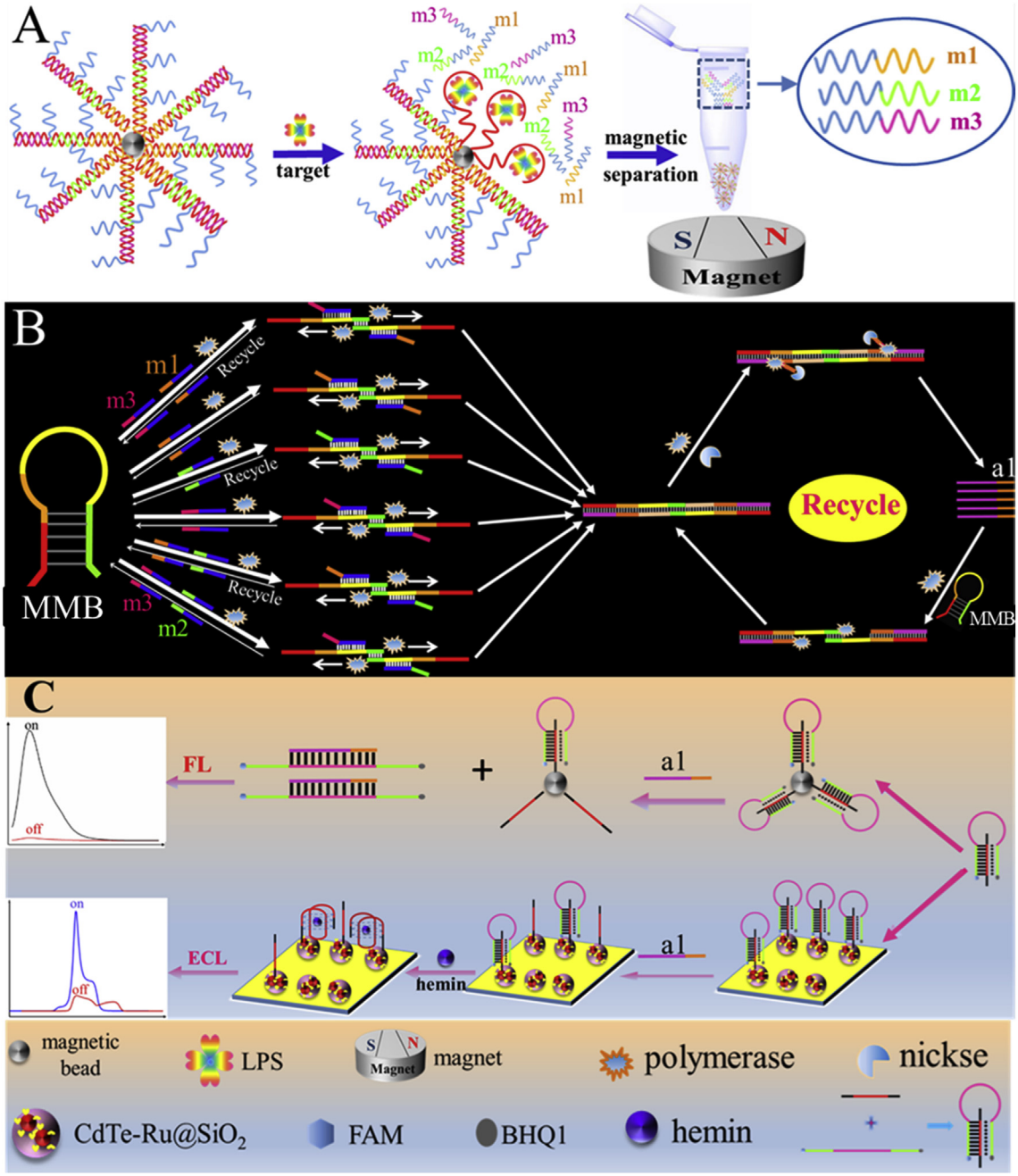

Scheme 1. Schematic illustration of the ECL and FL dual-signal biosensing platform for the detection of LPS by multiple-amplification process. (A) The release process of DNA sequences (m1, m2, m3) triggered by target LPS-aptamer binding on magnetic beads; (B) Multiple amplification cycle process for generating DNA fragments by MMB-m1 (or m2, m3) combination/polymerization/nicking; (C) Dual detection process of LPS by ECL "On-Off" and Fluorescence "Off-On" signals based on the triple helix molecular switch.

electrode shows a very high ECL signal in the detection buffer (curve a). When hemin is added to the detection buffer, the ECL signal slightly decreases due to the nonspecific adsorption of hemin on the modified electrode (curve b). When LPS is present, the specific LPS-aptamer binding induces release of DNA a1, then a1 opens the triple-helix DNA to expose mass G-rich DNA sequences S2, forming the hemin-quadruplex-hemin complex with adding hemin, which can greatly quench the ECL signal due to consumption of luminescent excitation state and increased electron transfer resistance (curve c). The results demonstrate that the present ECL strategy based on CdTe–Ru@SiO_2 and hemin/G-quadruplex can be used for signal "off" detection of target LPS.

3.6. PAGE analysis of the double amplification strategy

The biosensing platform consists of two amplification processes. The feasibility of the amplification strategy was investigated by polyacrylamide gel electrophoresis (PAGE) analysis. The concentration of target LPS is proportional to the amount of m1, m2, m3, which can be used for LPS detection. One target LPS can bind to its aptamer to release three DNA sequences (m1, m2, m3), which can amplify the signal (Scheme 1A). As shown in Fig. 3A, lane M is the marker, lanes a, b, c, and d are aptamers, m1, m2 and m3, respectively. Lane e is the aptamer-mDNAs, it migrates more slowly than the above DNA sequences, indicating the aptamer-m1, m2, m3 complexes are formed. After introducing LPS, it can be seen that m1, m2, m3 are released due to the

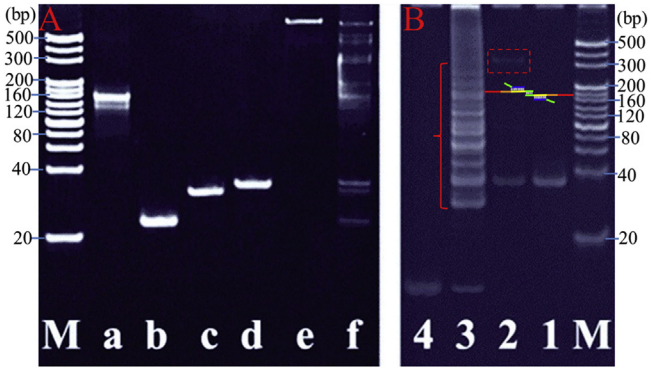

Fig. 3. PAGE analysis of the double amplification strategy: (A) The process of LPS-aptamer binding for inducing release of DNA sequences of m1, m2, m3, (B) Cyclic amplification process.

specific binding of LPS to aptamer (lane f), which can prove the LPS-induced amplification process.

Fig. 3B illustrates the feasibility of the cyclic amplification process. Lane M is the marker, lane 1 and lane 4 are MMB and a1, respectively. According to the principle of Scheme 1B, the hybridization of m1, m2, m3 with MMB is the same, any one of m1, m2, and m3 can be selected to characterize the hybridization by electrophoresis. Lane 2 is the hybrid result of MMB with m2, as the product has larger molecular weight and nearly 4-layer structure, so the steric hindrance is relatively large, leading to a relatively slow migration rate. The upper band (the dotted line in Fig. 3B) is the hybridization product, and the lower band is the superfluous MMB. After a series of polymerization and shearing reaction, large amounts of single strand DNA (a1) are released, corresponding to the lowest band in lane 3, which suggest the cyclic amplification process is performed. In addition, as many polymerization and shearing reaction processes at different stages were performed, the multiple bands in lane 3 (in bracket) are the intermediate products and redundant raw material DNA in the amplification process.

3.7. Electrochemical and ECL characterization of the ECL platform

In order to prove the stepwise fabrication of the ECL platform, the cyclic voltammogram (CV) is performed in 0.1 M PBS (pH 7.4) containing 5 mM $[Fe(CN)_6]^{3-/4-}$ (Fig. S3A). A pair of well-defined redox peaks of $[Fe(CN)_6]^{3-/4-}$ are observed on the bare GE (curve a). After modification of CdTe–Ru@SiO_2, the current decreases owing to the increased steric hindrance (curve b). When triple-helix DNA is linked to the CdTe–Ru@SiO_2 via amide bond, the peak current further decreases (curve c) because of the repellence between $[Fe(CN)_6]^{3-/4-}$ and negative charged DNA. Next, a consecutive decrease of the peak current is observed after blocking with the nonconductive MCH (curve d). When the prepared sensing surface is incubated with a1 solution, the triple-helix DNA is separated, so the peak current obviously increases (curve e). Sequentially, when hemin is present on the modified electrode, the redox peaks of hemin are observed (curve f). The CV profiles proved that the ECL biosensor was fabricated.

Moreover, ECL is also used to characterize different stages of the modified electrodes (Fig. S3B). A high ECL signal is observed from the CdTe–Ru@SiO_2 nanospheres (curve a), while the bare electrode almost displayed no ECL signal (curve f). When the triple-helix DNA is linked on the surface of the electrode, an obvious decrease of ECL intensity is observed due to the DNA molecule hindering to electron transfer (curve b). After blocking with MCH, the ECL sequentially decreased (curve c). When the modified electrode is further incubated with a1 solution, ECL intensity increased slightly (curve d). Sequentially, when hemin is dropped onto the modified electrode, a sharply reduced ECL intensity is seen (curve e), proving hemin quenched the ECL signal via competing coreactant and electron transfer mechanism. The results confirmed the ECL platform was successfully fabricated for LPS detection.

3.8. Optimization of experimental conditions

In order to achieve the best performance of the biosensing platform, the concentration of hemin, Klenow, and Nt.BbvCI are optimized. The reaction time of G-quadruplex-hemin complex, target cyclic amplification, and opening the triple helix structure are also studied with 1.0 pg/mL target LPS. Fig. S4A shows the ECL response to different concentration of hemin, the ECL intensity decreased with increasing hemin concentration, and reached a platform at 0.7 mM, indicating that 0.7 mM is the best concentration for the experiment.

Figs. S5A and S5B show the ECL responses to different concentration of Klenow and Nt.BbvCI. With the increasing concentration, the ECL signal responses gradually reduced, and did not change at 0.12 U/μL Klenow and 0.24 U/μL Nt.BbcCI, so 0.12 U/μL Klenow and 0.24 U/μL Nt.BbcCI were chosen in the biosensing platform.

Figs. S4B, S5C, and S5D show the reaction time of G-quadruplex-hemin complex, target cyclic amplification, and opening the triple helix structure. The ECL intensity decreased with increasing reaction time, and did not change at 30 min, 90 min, and 120 min, so these reaction time are selected as the optimal reaction conditions.

3.9. ECL detection of LPS with the biosensing platform by dual-amplification strategy

The ECL biosensing platform is used for detection of LPS. Under optimal reaction conditions, ECL responses to different concentrations of LPS were detected. When LPS concentrations increase from 0.1 fg/mL to 0.1 ng/mL, the ECL intensity gradually decreases (Fig. 4A), indicating that LPS concentration can be detected with the ECL biosensing platform.

Fig. 4B displays the relationship between the ECL signal change (ΔI_{ECL}) and LPS concentration, ΔI_{ECL} increases with increasing concentration of target LPS. Inset is the calibration curve for LPS detection with the biosensing platform, and a linear regression equation is obtained ($y = 1188.5\lg x + 3542.3$, $R^2 = 0.995$). The detection limit (LOD) is estimated to be 1.2×10^{-2} fg/mL ($3\sigma/N$, σ is the standard deviation of the blank and N is the slope of the corresponding calibration curve). The results demonstrate that the proposed ECL biosensing platform possess better performance for LPS detection with wide linear range and low detection limit compared to previous methods (Table S2).

3.10. Specificity and stability of the LPS biosensing platform

To evaluate the specificity of the biosensing platform for LPS assay, the ECL signal responses to the interference substances such as carcinoembryonic antigen (CEA), luteinizing hormone (LH), thrombin (TB), alpha fetoprotein (AFP) were detected. As shown in Fig. S6A, no significant ECL changes are observed in detecting interference substances compared with the blank. In contrast, significant ECL signal change is observed in the presence of LPS due to the specific recognition of LPS to aptamer, which suggests that the proposed biosensing platform possess high specificity for LPS detection.

Fig. S6B shows the ECL intensity under continuous scan for ten cycles by using 0.1 fg/mL LPS as a model, it can be seen that the biosensing platform exhibited good stability.

3.11. Fluorescence characterization of the triple helix DNA structure

In this study, FAM and BHQ as fluorophore and quencher were labeled at two ends of S1 chain. As shown in Fig. S7, in the absence of DNA S2, the fluorescence intensity of DNA S1 is high (4607 au, curve a). However, when DNA S2 is present, the intermolecular DNA hybridization of S1 with S2 induced by Watson-Crick and Hoogsteen base

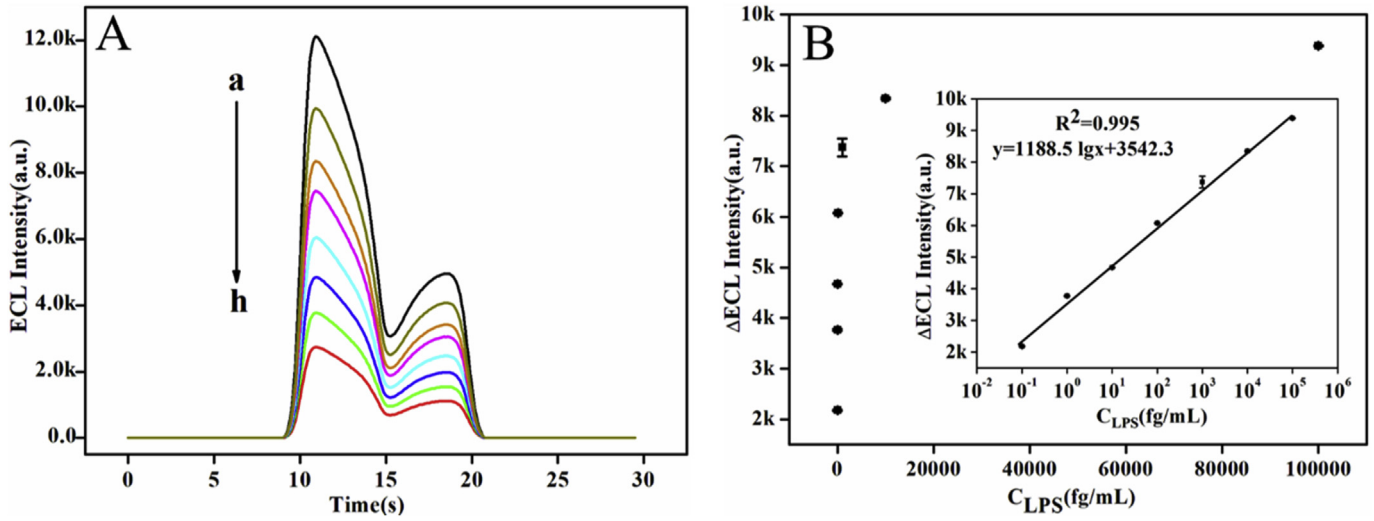

Fig. 4. (A) ECL signals of the biosensing platform to increasing concentrations of target LPS (fg/mL): (a) 0; (b) 0.1; (c) 1.0; (d) 10; (e) 100; (f) 1000; (g) 10000; (h) 100000 (from a to h). (B) Relationship between ΔECL (deducting background, $\Delta I_{ECL} = I_0 - I_n$) and LPS concentration (inset: the logarithmic calibration plot for LPS detection), error bars represent standard deviations of three parallel experiments.

pairing was performed, the FAM fluorophore and BHQ quencher are close, so the fluorescence signal is quenched (curve b), indicating that the triple-helix structure was formed.

3.12. FL detection of LPS with the biosensing platform by dual-amplification strategy

Under the optimized conditions, the feasibility of the biosensing platform for FL detection of LPS was investigated. As shown in Fig. 5A, the background fluorescence intensity (in the absence of target LPS) is very low (204 au, curve a). However, when the target LPS is present, the fluorescence signals are obviously high, and gradually increase with LPS concentration from 10 fg/mL to 1.0 μg/mL (curve b to j), suggesting that the present biosensing platform can be used for FL detection of LPS.

Fig. 5B displays the relation curve between the fluorescence signal changes and LPS concentration for target detection (inset: calibration plot for LPS detection), the changes of fluorescence signal (ΔI_{FL}) shows a linear relation with LPS concentration, and the regression equation is $y = 366.3 \lg x + 2223.1$ ($R^2 = 0.994$). A detection limit (LOD) is estimated to be 1.269 fg/mL (3σ/N), which is lower than those in the previous report (Table S2), demonstrating that the FL biosensing platform shows good performance.

3.13. Specificity of the FL biosensing platform

The specificity of the FL biosensing platform for LPS assay was evaluated. As shown in Fig. S9, non-target analytes (CEA, LH, TB, AFP) did not cause significant influence on FL intensity. In contrast, significant FL increment was observed in the presence of LPS, suggesting that the proposed FL biosensing platform hold high specificity for LPS detection.

4. Conclusions

In summary, a novel biosensing platform with dual-amplification and dual-signal was proposed for ultrasensitive determination of LPS on the basis of the triple-helix molecular switch. Several advantages of the strategy have been demonstrated. First, a novel CdTe–Ru@SiO_2 nanospheres/TPrA-based ECL platform is constructed, which is used to realize "On − Off" signal response for target assay by a triple-helix molecular switch and hemin. Second, the dual-amplification process and dual-signal mode are reported for ultrasensitive detection of LPS for the first time. Moreover, in comparison with traditional biological detection methods, the developed biosensing platform exhibited excellent performance with higher sensitivity, selectivity, wider linear ranges,

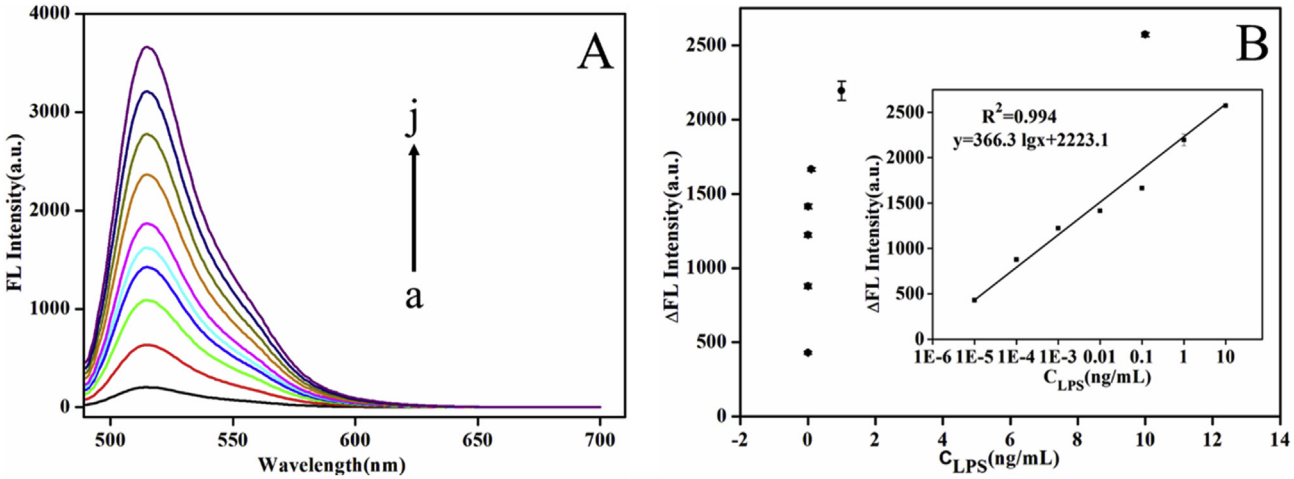

Fig. 5. (A) Fluorescence signal responses for detection of different concentrations of LPS (ng/mL): (a) 0; (b) 0.00001; (c) 0.0001; (d) 0.001; (e) 0.01; (f) 0.1; (g)1.0; (h) 10; (i) 100; (j) 1000 (from a to j). (B) Relation of the fluorescence signal changes with LPS concentration (inset: calibration plot for LPS detection).

and lower detection limits, which has promising applications in clinical diagnosis.

Conflict of interest

There is no conflict to declare.

CRediT authorship contribution statement

Xiaoshan Gao: Writing - original draft. **Hongkun Li:** Data curation. **Yu Zhao:** Writing - review & editing. **Guifen Jie:** Writing - original draft, Formal analysis.

Acknowledgements

This work was supported by the National Natural Science Foundation of China (No. 21575072).

Appendix A. Supplementary data

Supplementary data to this article can be found online at https://doi.org/10.1016/j.bios.2019.111602.

References

Cai, F.D., Zhu, Q., Zhao, K., Deng, A.P., Li, J.G., 2015. Environ. Sci. Technol. 49, 5013–5020.
Carrara, S., Arcudi, F., Prato, M., Cola, L.D., 2017. Angew. Chem. Int. Ed. 56, 4757–4761.
Chang, S.Q., Wu, X., Lan, J.Z., Li, Z., Zhang, X.H., Zhang, H.Q., 2019. Nanomaterials 9, 506.
Cho, M.S., Lee, S.C., Chae, H.J., Kwon, Y.M., Kim, H.J., Ryu, M.Y., Lee, J.B., Kim, J.C., 2019. Renew. Energy 144, 107–115.
Dong, Y.P., Gao, T.T., Zhou, Y., Jiang, L.P., Zhu, J.J., 2015. Sci. Rep. 5, 15392.
Du, Y., Dong, S., 2017. Anal. Chem. 89, 189–215.
Ge, J.J., Zhao, Y., Li, C.L., Jie, G.F., 2019a. Anal. Chem. 91, 3546–3554.
Ge, J.J., Li, C.L., Zhao, Y., Yu, X.J., Jie, G.F., 2019b. Chem. Commun. 55, 7350–7353.
Gu, Z., Zou, L., Fang, Z., Zhou, W., Zhong, X., 2008. Nanotechnology 19, 135604.
Jie, G.F., Ge, J.J., Gao, X.S., Li, C.L., 2018. Biosens. Bioelectron. 118, 115–121.
Khonsari, Y.N., Sun, S., 2017. Chem. Commun. 53, 9042–9054.
Khonsari, Y.N., Sun, S., 2018. Microchimica Acta 185, 430.
Lee, L.G., Connell, C.R., Bloch, W., 1993. Nucleic Acids Res. 21, 3761–3766.
Li, L., Chen, Y., Zhu, J.J., 2017. Anal. Chem. 89, 358–371.
Li, L.L., Zhang, Z.Y., Chen, Y., Xu, Q., Zhang, J.-R., Chen, Z.X., Chen, Y., Zhu, J.-J., 2019. Adv. Funct. Mater. 1902533.
Liang, W.B., Zhuo, Y., Xiong, C.Y., Zheng, Y.N., Chai, Y.Q., Yuan, R., 2015. Anal. Chem. 87, 12363–12371.
Liu, J., Lu, Y., 2006. Nat. Protoc. 1, 246–252.
Liu, X., Lu, C.H., Willner, I., 2014. Acc. Chem. Res. 47, 1673–1680.
Liu, Z.Y., Qi, W.J., Xu, G.B., 2015. Chem. Soc. Rev. 44, 3117–3142.
Miao, W., Choi, J., Bard, A.J., 2002. J. Am. Chem. Soc. 124, 14478–14485.
Omberg, K.M., Schoonover, J.R., Treadway, J.A., Leasure, R.M., Dyer, R.B., Meyer, T.J., 1997. J. Am. Chem. Soc. 119, 7013–7018.
Rangin, M., Basu, A., 2004. J. Am. Chem. Soc. 126, 5038–5039.
Swanick, K.N., Ladouceur, S., Zysman-Colman, E., Ding, Z., 2012. Angew. Chem. Int. Ed. 51, 11079–11082.
Torring, T., Voigt, N.V., Nangreave, J., Yan, H., Gothelf, K.V., 2011. Chem. Soc. Rev. 40, 5636–5646.
Ulevitch, R.J., Tobias, P.S., 1994. Curr. Opin. Immunol. 6, 125–130.
Voss, S., Fischer, R., Jung, G., Wiesmüller, K.H., Brock, R., 2007. J. Am. Chem. Soc. 129, 554–561.
Wang, F., Liu, X., Willner, I., 2015. Angew. Chem. Int. Ed. 54, 1098–1129.
Wang, H.J., Yuan, Y.L., Zhuo, Y., Chai, Y.Q., Yuan, R., 2016a. Anal. Chem. 88, 2258–2265.
Wang, T., Wang, D., Padelford, J.W., Jiang, J., Wang, G., 2016b. J. Am. Chem. Soc. 138, 6380–6383.
Wang, Q., Chen, M., Zhang, H., Wen, W., Zhang, X., Wang, S., 2016c. Sens. Actuators, B 222, 264–269.
Warren, H.S., Fitting, C., Hoff, E., Adib-Conquy, M., Beasley-Topliffe, L., Tesini, B., Liang, X., Valentine, C., Hellman, J., Hayden, D., Cavaillon, J.M., 2010. J. Infect. Dis. 201, 223–232.
Wen, W., Yan, X., Zhu, C., Du, D., Lin, Y., 2017. Anal. Chem. 89, 138–156.
Wilner, O.I., Willner, I., 2012. Chem. Rev. 112, 2528–2556.
Willner, I., Shlyahovsky, B., Zayats, M., Willner, B., 2008. Chem. Soc. Rev. 37, 1153–1165.
Yu, T., Dai, P.P., Xu, J.J., Chen, H.Y., 2016. ACS Appl. Mater. Interfaces 8, 4434–4441.
Zhang, D.Y., Seelig, G., 2011. Nat. Chem. 3, 103–113.
Zhang, L., Dong, S., 2006. Anal. Chem. 78, 5119–5123.
Zain, R., Sun, J.S., 2003. Cell. Mol. Life Sci. 60, 862–870.
Zhang, X., Tan, X., Zhang, B., Miao, W.J., Zou, G.Z., 2016. Anal. Chem. 88, 6947–6953.
Zhao, M., Chen, A.Y., Dan, H., Chai, Y.Q., Zhuo, Y., Yuan, R., 2017. Anal. Chem. 89, 8335–8342.
Zhuo, Y., Liao, N., Chai, Y.Q., Gui, G.F., Zhao, M., Han, J., Xiang, Y., Yuan, R., 2014. Anal. Chem. 86, 1053–1060.